TOTEM Note 2006-002
3 May 2007

Algebraic Determination of Roman Pot Acceptance and Resolution for the $\beta^* = 1540\,\mathrm{m}$ Optics

M. Deile

Abstract

This note describes algebraic methods for calculating Roman Pot acceptance and reconstruction resolution in the kinematic variables of diffractively scattered protons. This approach being based on a parameterisation [1] of the optical functions for $\beta^* = 1540\,\mathrm{m}$, results are obtained rather fast without tracking individual protons through the LHC ring. Evidently, the precision of the results relies on the accuracy of the parameterisation.

Slight differences between the results in this note and the ones given in the (older) CMS/TOTEM physics TDR [2] are due to the correction of some suboptimal program features.

1 Introduction

A proton produced in a diffractive interaction with the kinematic parameters t, ϕ, ξ, x^*, y^*, passes a Roman Pot (RP) detector plane i at a position (x_i, y_i) determined by the beam optics between the interaction point and the RP. For describing the proton's transport, it is convenient to reparameterise its kinematics in terms of ξ and the orthogonal projections of the scattering angle, θ_x and θ_y.
Using basic kinematics starting from the definition

$$t = (E - E')^2 - (\vec{p} - \vec{p}')^2 \tag{1}$$

where the primed variables denote the quantities after the interaction, t can be expressed in terms of the scattering angle θ, the initial momentum p, the proton mass m and the fractional momentum loss $\xi = \frac{p-p'}{p}$:

$$-t = -t_0 + 4p^2(1-\xi)\sin^2\frac{\theta}{2} \tag{2}$$

with the kinematic limit

$$-t_0 = 2\left(p^2 + m^2\right)\left[\sqrt{1 + \frac{p^2(\xi^2 - 2\xi)}{p^2 + m^2}} - 1\right] + 2\xi p^2\,. \tag{3}$$

Hence, in the general case, t and ξ cannot be considered as independent variables. Far away from the kinematic limit however, i.e. for $-t \gg -t_0$ and $\xi \ll 1$, this expression reduces to the more familiar approximation

$$-t \approx p^2\theta^2 \quad \text{or} \quad \theta = \frac{-t}{p}\,. \tag{4}$$

Finally, we write

$$\theta_x = \theta \cos\phi \quad (5)$$
$$\theta_y = \theta \sin\phi\,. \quad (6)$$

Using the parametrisation of the optical functions given in [1], the vectors (or sets) $\vec{x}$ and $\vec{y}$ of the proton's position measurements x_i and y_i in the RP units at the positions z_i can be expressed by the matrix equations

$$\vec{x} = H_x(\vec{\Xi}_x)\,\vec{\Xi}_x + \delta\vec{x}\,, \quad (7)$$
$$\vec{y} = H_y(\vec{\Xi}_x, \vec{\Xi}_y)\,\vec{\Xi}_y + \delta\vec{y}\,, \quad (8)$$

where the kinematic variables relevant for the x- and y-projection are also combined in vector notation:

$$\vec{\Xi}_x = \begin{pmatrix} \theta_x \\ \xi \\ x^* \end{pmatrix} \text{ and } \vec{\Xi}_y = \begin{pmatrix} \theta_y \\ y^* \end{pmatrix}\,. \quad (9)$$

The transport matrices are given by

$$H_x(\vec{\Xi}_x) = \left(\vec{L}_x(\xi),\ \vec{D}(\theta_x, \xi, x^*),\ \vec{v}_x(\xi)\right) \text{ and} \quad (10)$$
$$H_y(\vec{\Xi}_x, \vec{\Xi}_y) = \left(\vec{L}_y(\xi),\ \vec{v}_y(\xi)\right)\,, \quad (11)$$

where the vectors $\vec{L}_x$ etc. contain the optical functions at the measurement positions z_i. H_x and H_y depend on the kinematics, introducing non-linearity to the system.
Due to the finite detector resolution, the measurements $\vec{x}$ and $\vec{y}$ are shifted randomly by $\delta\vec{x}$ and $\delta\vec{y}$. Additional smearing is caused by the beam energy uncertainty and the angular divergence as given in Table 1.

Table 1: *Beam parameters with the β^*=1540 m optics at the reduced emittance ε=1 μm·rad. A beam energy spread of 10^{-4} is assumed.*

Energy Spread	Crossing Angle [μrad]	IP Offset in x [μm]	IP Beam Size [μm]	IP Beam Divergence [μrad]
10^{-4}	0	0	450	0.3

2 Acceptance in ξ and t

To obtain a fully detailed and precise evaluation of the RP detector acceptance, protons with given kinematic variables have to be tracked along the LHC ring with MAD-X, as described in [3]. However, a very reasonable approximation can be achieved by replacing the tracking simulation with the parameterisation of the optical functions. The main advantage is the considerable reduction of computing time, allowing a much finer binning in the kinematic variables. Considering that the finite width of the vertex position (x^*, y^*) would just smear the equiacceptance contour lines, we only treat the case of the mean vertex $(x^*, y^*) = (0, 0)$. The algorithm proceeds as follows:

- Generation of protons by looping over values of $\lg(-t)$, $\lg\xi$, ϕ in equidistant steps over intervals of interest. The kinematic limit (3) is taken into account.

- Calculation of the positions (x_i, y_i) in RP plane i using the parameterisation of the optical functions.
- Comparison of (x_i, y_i) with the RP detector area (Figure 1): if the point lies inside this area, the 3-dimensional binary acceptance $A(\lg(-t), \lg\xi, \phi) = 1$, otherwise 0. This is done separately for horizontal and vertical detectors.
- Further acceptance test at the aperture limiting elements along the trajectory from the IP to the RP (quadrupoles, beam screens etc.) using the values of r_{max} and d_{max} from Table 1 in [1] together with the optical functions at the positions of these elements.
- Logical combinations of the 3-dimensional binary acceptances:
  - $A = A_1 \,|\, A_2$ to combine RP detectors in the same unit.
  - $A = A_1 \,\&\, A_2$ to build the coincidence between different RP stations.
- Projection onto a kinematic subspace (usually $(\lg(-t), \lg\xi)$).

The results in $(\lg(-t), \lg\xi)$ are shown in Figure 2 for the RP station at 145 m, in Figure 3 for the station at 220 m, and in Figure 4 for the coincidence of both.

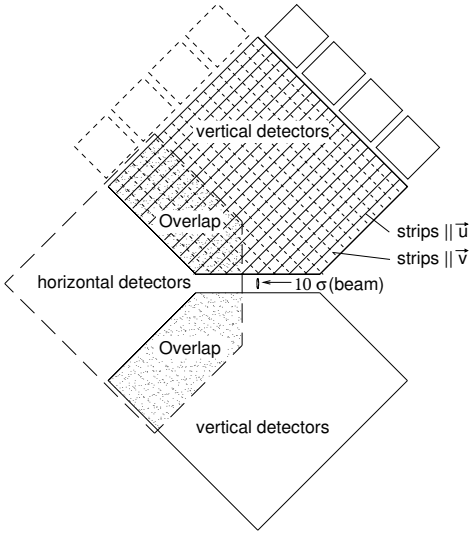

Figure 1: *Geometry of the detectors in one RP unit. The detectors approach the beam to* $10\,\sigma + 0.5\,\text{mm}$.

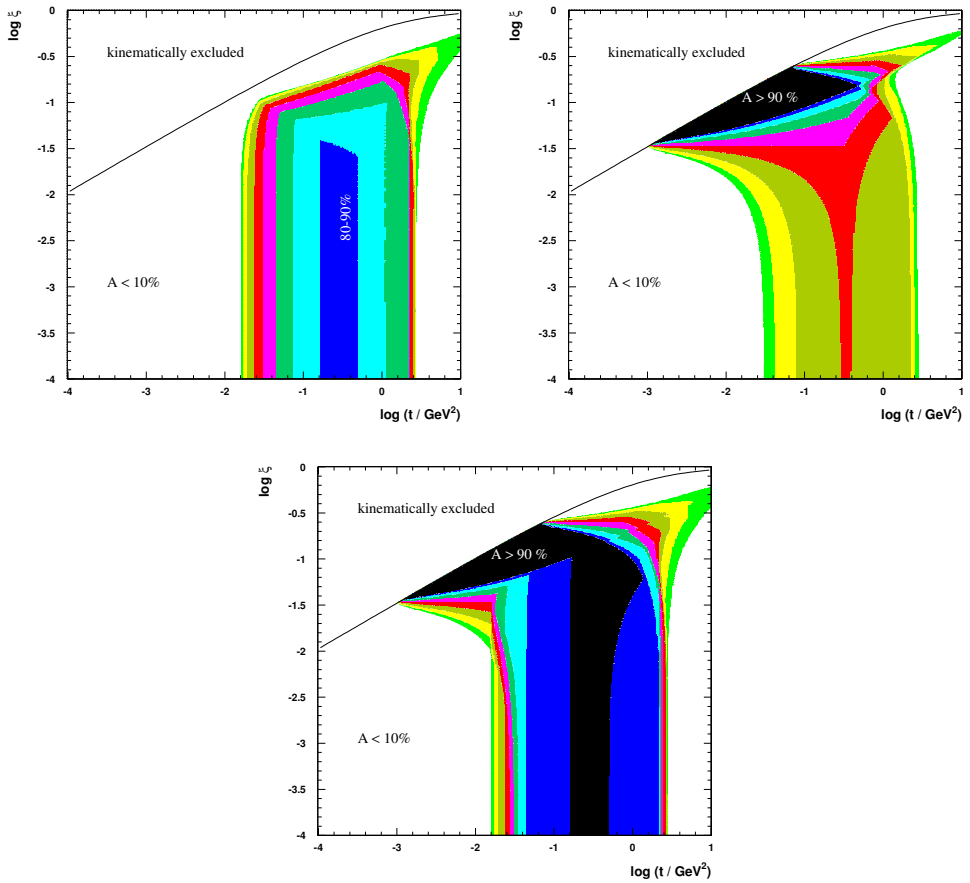

Figure 2: *Acceptance for diffractive protons in t and ξ for the RP145 station; left: vertical detectors; right: horizontal detectors; bottom: all 3 detectors combined.*

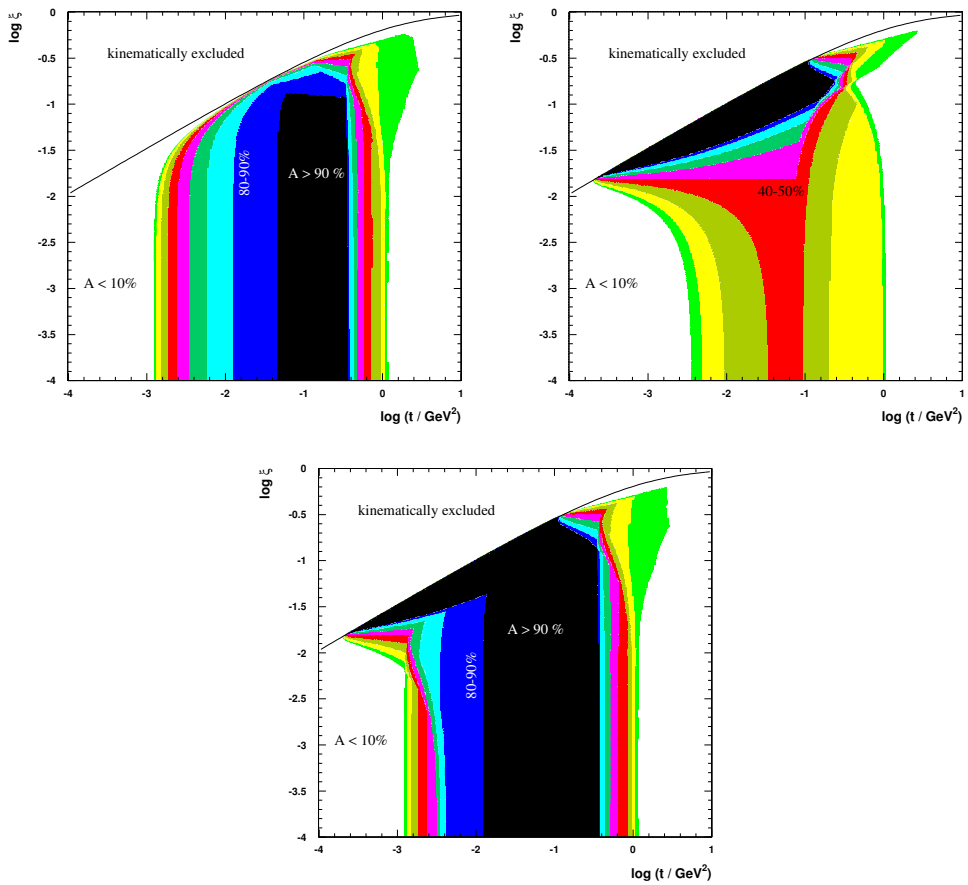

Figure 3: *Acceptance for diffractive protons in t and ξ for the RP220 station; left: vertical detectors; right: horizontal detectors; bottom: all 3 detectors combined.*

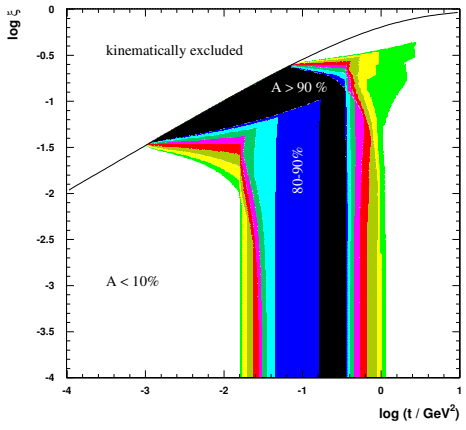

Figure 4: *Acceptance for diffractive protons in t and ξ using the RPs at 145 m and 220 m in coincidence.*

3 Reconstruction of the Kinematic Variables

3.1 Reconstruction Method

The reconstruction procedure described in this section aims at the determination of the kinematic parameters $\theta_{x,y}$, ξ of the proton. Since the large beam size at the IP characterising the β^*=1540 m optics does not allow to neglect the vertex contribution, the vertex coordinates (x^*, y^*) are treated as additional free variables. The reconstruction task therefore consists in resolving Eqns. (7) and (8) for $\vec{\Xi}_x$ and $\vec{\Xi}_y$. To obtain a unique solution including the vertex, at least 3 position measurements are needed which is not possible with the 216/220 m RP station alone. Inclusion of the 145/149 m station brings the number of equations to 4, but it has the disadvantage of a reduced acceptance in t; cf. Figure 3 and Figure 4.
By largely renouncing the vertex reconstruction, however, the matrix equation can be formally solved even without the 145/149 m station. Technically, a weak constraint from the knowledge of the beam width σ_{beam} at the vertex is introduced. The unbiassed estimate $x_0 \equiv \hat{x}^* = 0$ with the (big) uncertainty given by the interaction width $\sigma(x_0) = \sigma_{beam}/\sqrt{2} = 0.45\,\mathrm{mm}/\sqrt{2} = 0.32\,\mathrm{mm}$ (and analogously for y) can play the role of a measurement contributing another row to each of the matrix equations (7) and (8) with optical parameters $L_{x0} = L_{y0} = 0$, $D_0 = 0$, $v_{x0} = v_{y0} = 1$.
Since this vertex constraint always adds some information, we use it even in the reconstruction with 4 RP units.

Without the dependence of the optical functions on the kinematics, the algebraic inversion problem would be linear and could be solved analytically. Describing the measurement resolution by the diagonal covariance matrices

$$V_x = \begin{pmatrix} \sigma_{x1}^2 & & O \\ & \ddots & \\ O & & \sigma_{xn}^2 \end{pmatrix}, \; V_y = \begin{pmatrix} \sigma_{y1}^2 & & O \\ & \ddots & \\ O & & \sigma_{yn}^2 \end{pmatrix}, \tag{12}$$

the best estimator for $\vec{\Xi}_x$ is given by

$$\hat{\vec{\Xi}}_x = \left(H_x^T V_x^{-1} H_x\right)^{-1} H_x^T V_x^{-1} \vec{x} \tag{13}$$

(analogously for $\hat{\vec{\Xi}}_y$), and its covariance matrix by

$$U_x = \left(H_x^T V_x^{-1} H_x\right)^{-1} . \tag{14}$$

To take into account the non-linearity, two procedures are possible:

1. Iterative reconstruction using Eqn. (13), evaluating the transport matrices at the current estimates $\vec{\Xi}_x^{(k)}$ and $\vec{\Xi}_y^{(k)}$ in each step k.

2. Solution of Eqns. (7) and (8) by minimisation of

$$\chi^2 = \sum_i \frac{\left(x_i - [H_x(\vec{\Xi}_x)\,\vec{\Xi}_x]_i\right)^2}{\sigma_{xi}^2} + \sum_i \frac{\left(y_i - [H_y(\vec{\Xi}_x, \vec{\Xi}_y)\,\vec{\Xi}_y]_i\right)^2}{\sigma_{yi}^2} \tag{15}$$

It was observed that approach 1 with typically 10 iterations yields the same result as approach 2. All detailed studies below were performed with approach 2.

Note that the reconstructed kinematic quantities differ from the ones relevant for the diffractive process due to the beam energy uncertainty and the angular divergence (Table 1). The reconstruction of the scattering angle will yield the angle between the outcoming proton and the ideal beam angle, whereas for the momentum transfer the actual beam angle would be relevant. Similarly, the ξ reconstruction is based on the assumption of an incoming proton with 7 TeV. The resolutions obtained in the studies below have been corrected accordingly.
Systematic effects from errors in the alignment of the detectors with respect to the beam have not been considered in the present study. Furthermore, in the case where several RP stations are used, multiple scattering in the upstream units will affect the trajectories through the downstream units. This effect has not been included yet.

3.2 Single-Arm Reconstruction (SD)

The reconstruction of single protons has been evaluated

- using only the RP units at 216 m and 220 m;
- using the units at 145 m, 149 m, 216 m and 220 m.

The resolution studies were performed first on events generated with the parametrisation of the optical functions. This ideal case, where the optics are perfectly known, shows the intrinsic performance of the reconstruction method and hence yields a lower limit on the achievable resolution. Then, as a second step, the protons were taken from DPE events generated with PHOJET and tracked through the machine with MAD-X. In this approach, the performance is deteriorated by imperfections in the parametrisation of the optics and hence corresponds better to reality where the optics are not precisely known.

3.2.1 Ideal Study with Perfectly Known Optics

For each set of kinematic variables, 10000 protons were generated with randomised vertex positions ($\sigma(x^*) = \sigma(y^*) = 0.32\,\text{mm}$), beam angles ($\sigma(\theta_{beam}) = 0.29\,\mu\text{rad}$) and beam momentum ($\sigma(p_{beam})/p_{beam} = 10^{-4}$). The hit positions in the detectors were calculated with the optics parametrisation and then smeared with the detector resolution of 20 μm. Then the reconstruction was done with a fit as described above, using again the optics parametrisation. The resolutions in ξ and t were then defined as the standard deviations of the distributions of $\Delta\xi = \xi - \xi_{true}$ and $\Delta t = t - t_{true}$. They are shown in Figures 5 and 6 respectively. The results for all the other kinematical parameters are given in Figures 7 to 9. The curves for $\phi = \pi$, where there is no acceptance, are only given for completeness. At large ξ (> 0.01) the deviation distributions become very non-gaussian and acquire tails which makes the quantification of their widths difficult. Furthermore, there are difficulties at very small $|t|$ where the Δt distribution is truncated and hence very non-gaussian. There the ϕ-resolution is bad too.
If only the RPs at 216 m and 220 m are used (top plots), the ξ-resolution is significantly worse than if all RPs are used (bottom plots). In the latter case the tracks are measured before and after the dipole D2 which thus acts as a spectrometer.
The difference in resolution between the horizontal directions $\phi = 0$ and π stems from the dependence of the dispersion on θ_x.

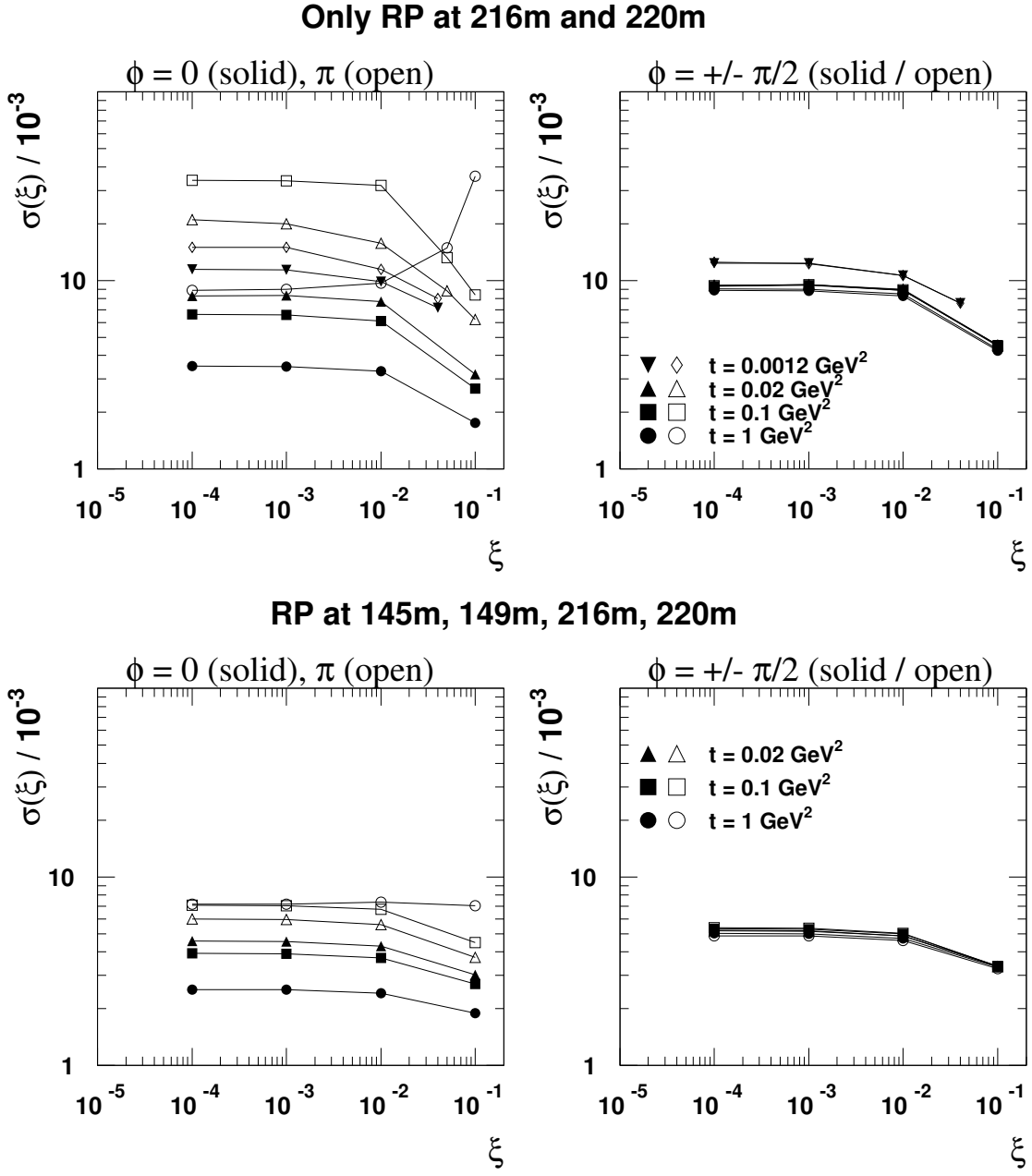

Figure 5: *ξ resolution with perfectly known optics as a function of ξ for different t and azimuthal angles: $\phi = 0, \pi$ (left-hand plots), i.e. horizontal, and $\phi = \pm\pi/2$ (right-hand plots), i.e. vertical.*

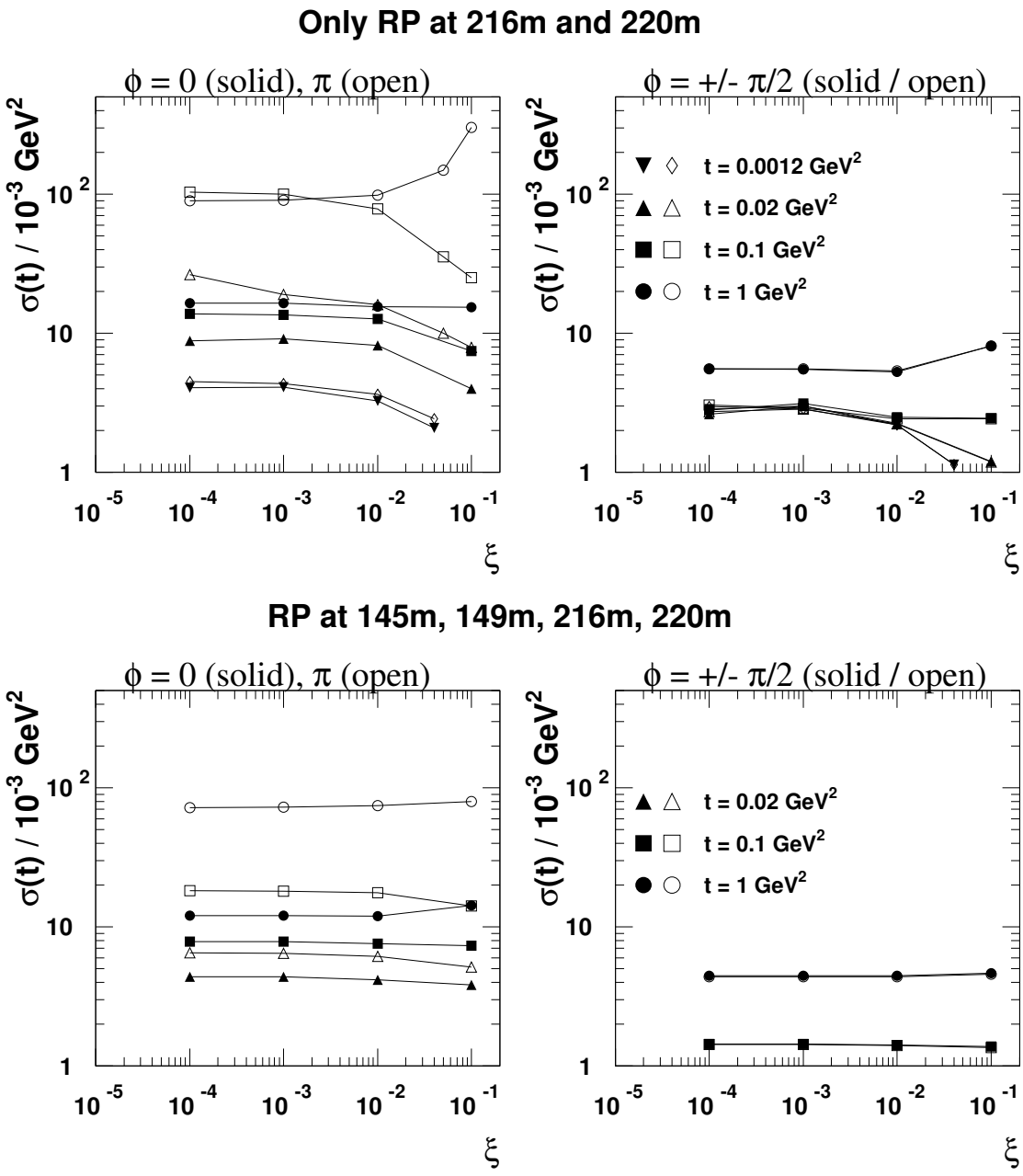

Figure 6: *t resolution with perfectly known optics as a function of ξ for different t and azimuthal angles: $\phi = 0, \pi$ (left-hand plots), i.e. horizontal, and $\phi = \pm\pi/2$ (right-hand plots), i.e. vertical.*

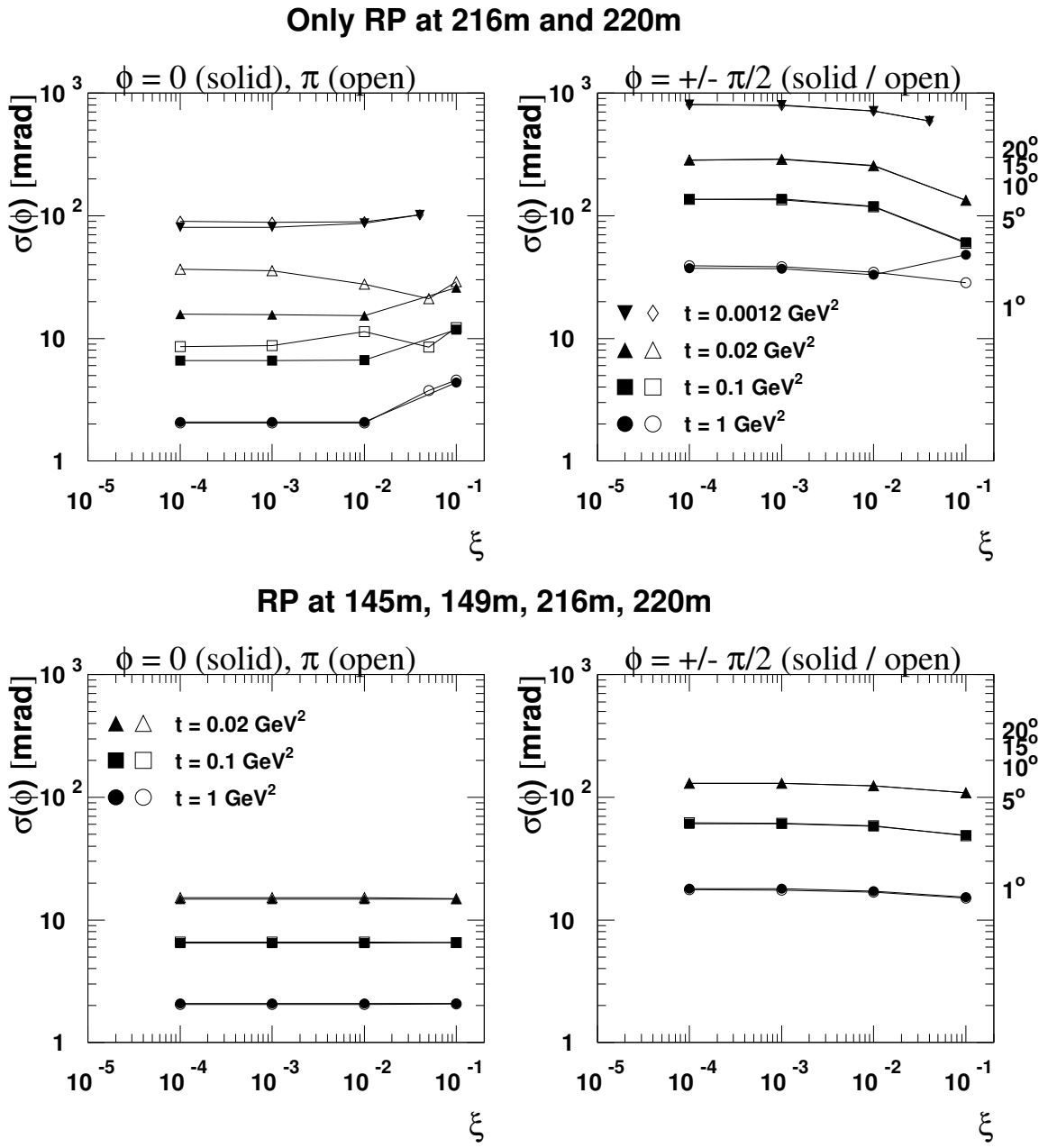

Figure 7: *ϕ resolution with perfectly known optics as a function of ξ for different t and azimuthal angles.*

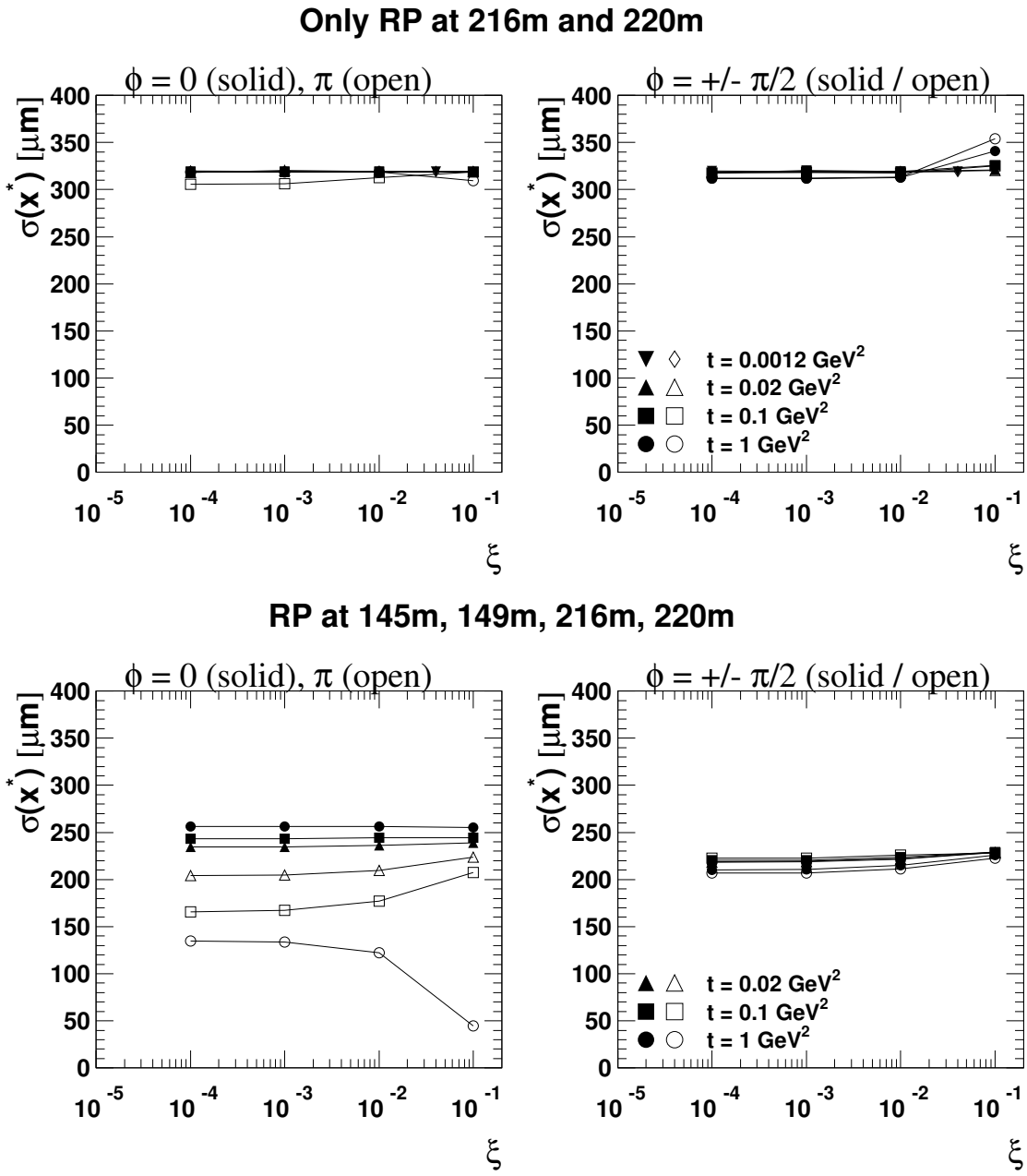

Figure 8: *x^* resolution with perfectly known optics as a function of ξ for different t and azimuthal angles.*

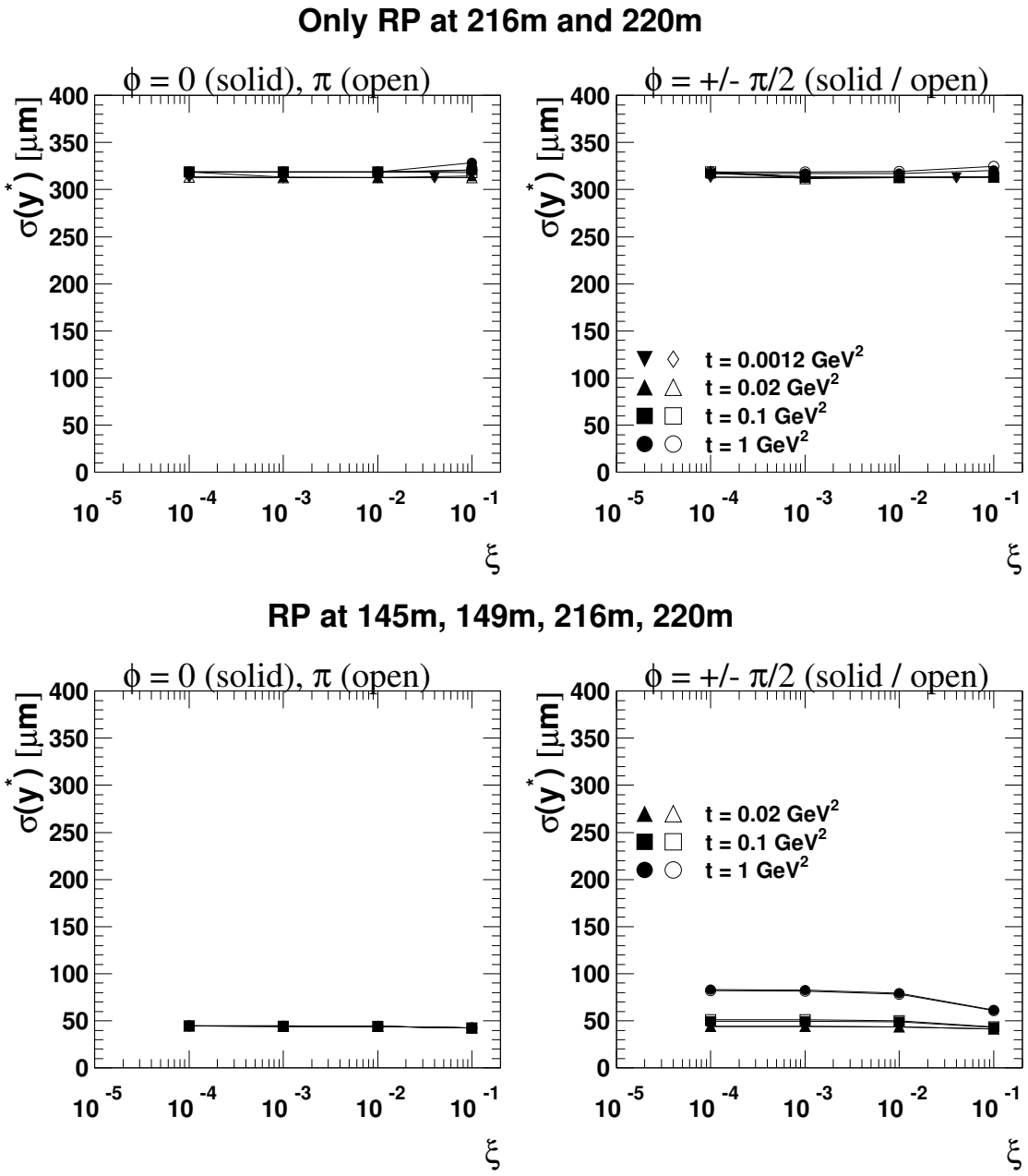

Figure 9: *y^* resolution with perfectly known optics as a function of ξ for different t and azimuthal angles.*

3.2.2 Study Based on Protons Tracked through the Machine

A sample of protons from 10000 DPE events generated with PHOJET was tracked through the machine with MAD-X. Like in the previous study, the vertex positions, beam angles, beam energies and hit positions in the detectors were smeared. The reconstruction was again done with a fit based on the optics parametrisation. The results are shown in Figures 10 to 14 for the different parameters in intervals of t and ξ.

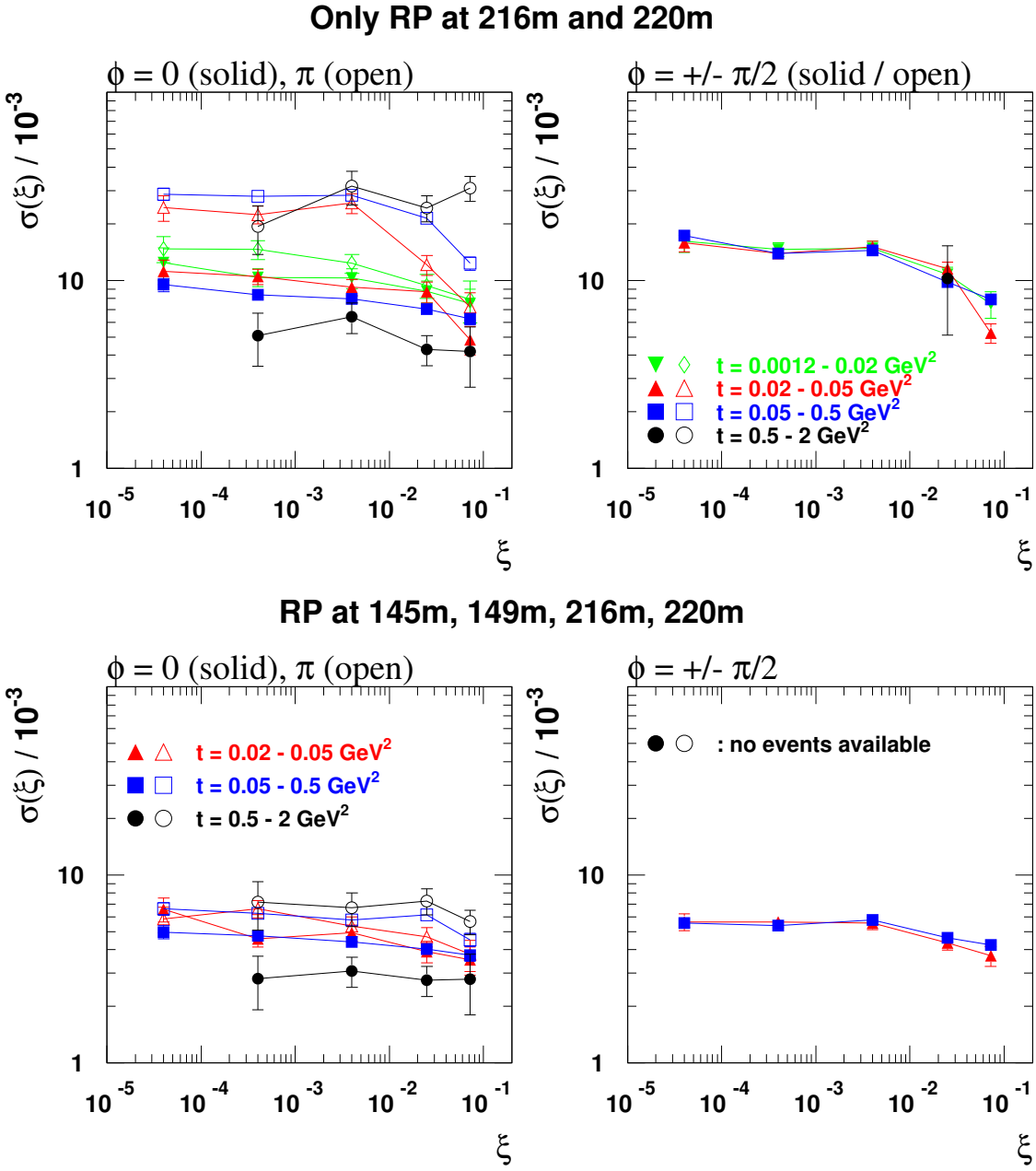

Figure 10: *ξ resolution with tracked protons as a function of ξ for different t and azimuthal angles: $\phi = 0, \pi$ (left-hand plots), i.e. horizontal, and $\phi = \pm\pi/2$ (right-hand plots), i.e. vertical.*

Deviations from the performance with perfectly known optics occur in cases where the parametrisation is not accurate enough. Such situations are not only characterised by a

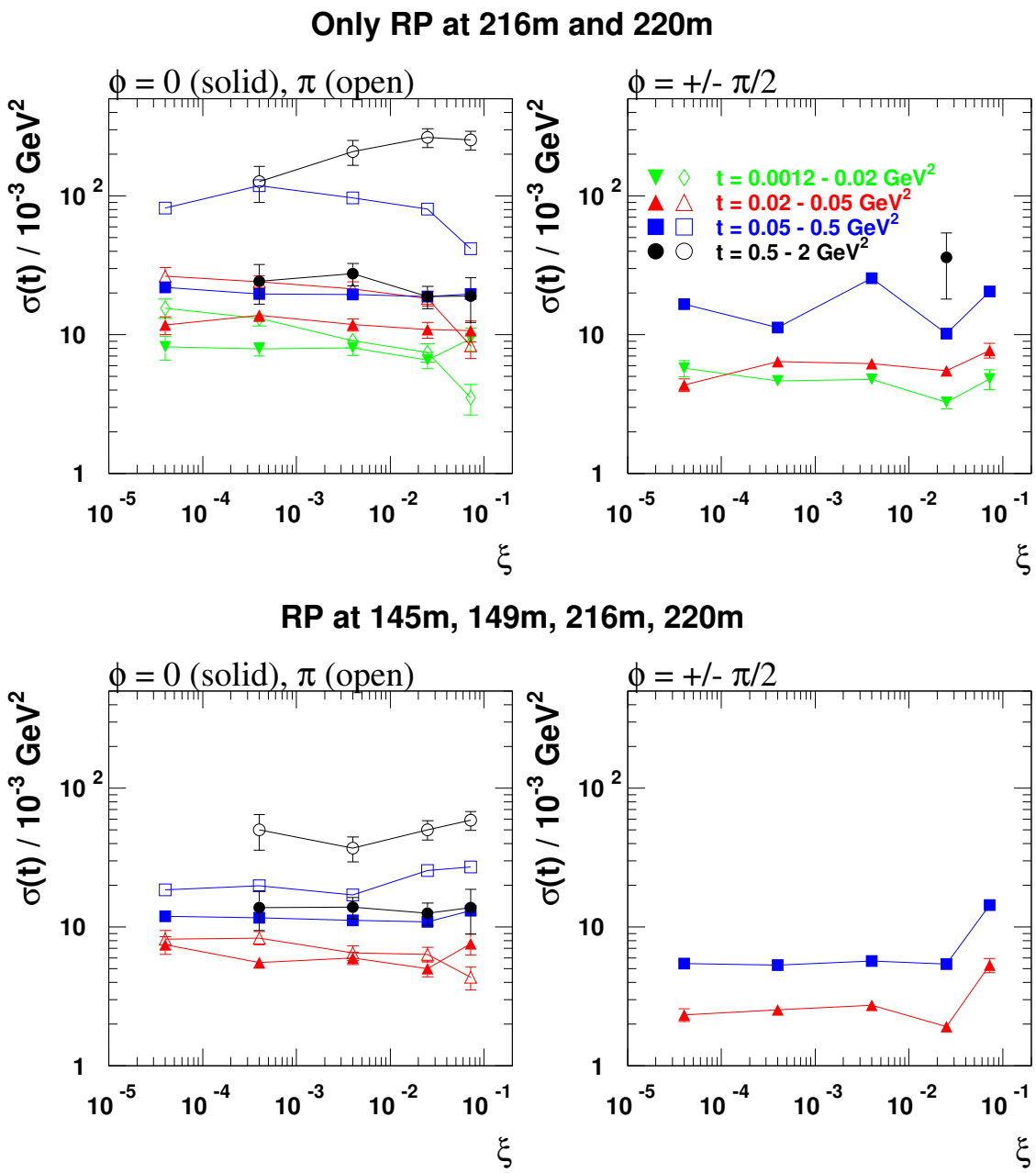

Figure 11: *t resolution with tracked protons as a function of ξ for different t and azimuthal angles: $\phi = 0, \pi$ (left-hand plots), i.e. horizontal, and $\phi = \pm\pi/2$ (right-hand plots), i.e. vertical.*

worse resolution but also by reconstruction biases which are not observed in the case of perfectly known optics. Furthermore, many (ξ, t) slices in the real-proton study suffer from very poor statistics as can be seen from large error bars or steps in the curves.

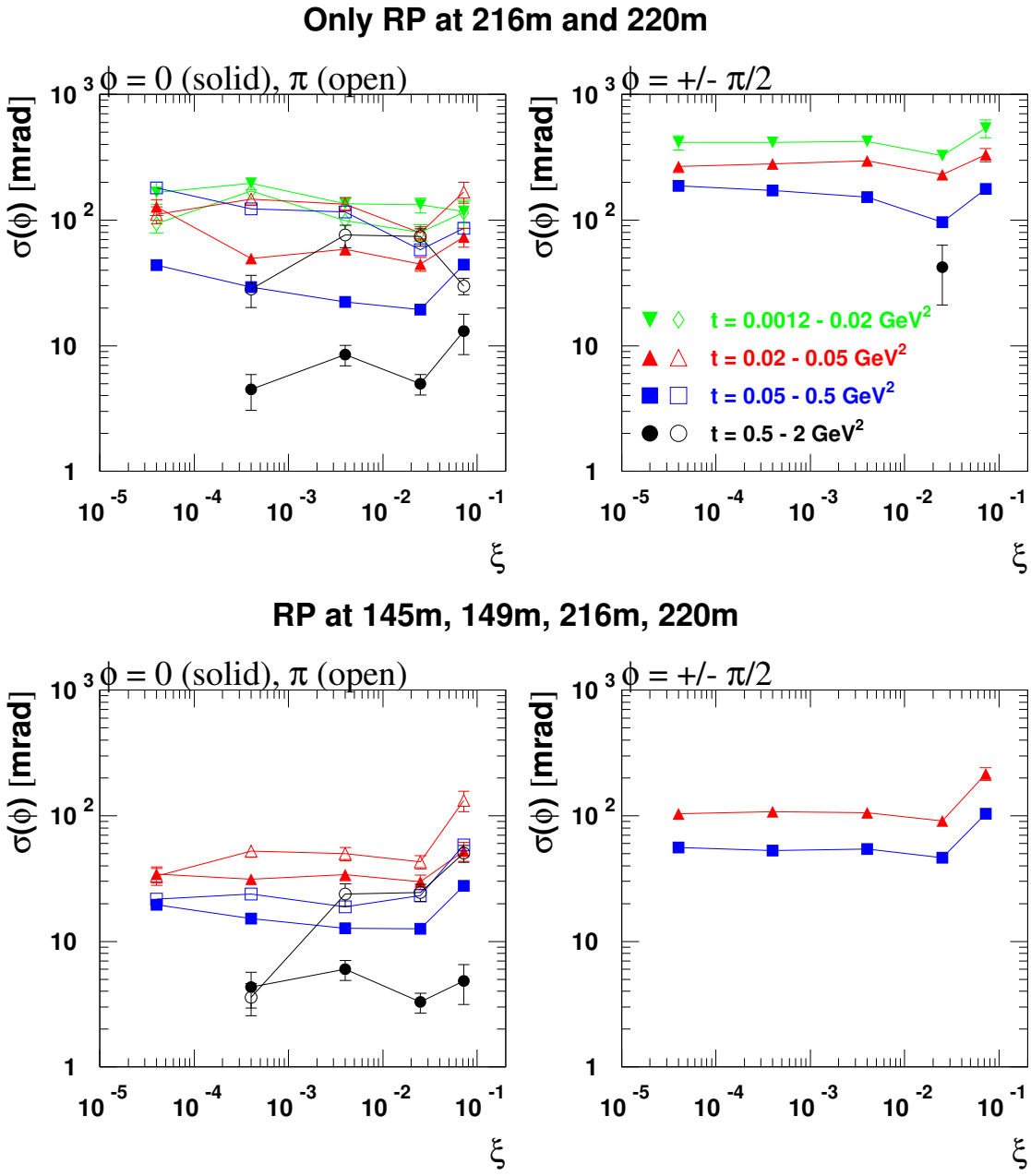

Figure 12: *ϕ resolution with tracked protons as a function of ξ for different t and azimuthal angles: $\phi = 0, \pi$ (left-hand plots), i.e. horizontal, and $\phi = \pm\pi/2$ (right-hand plots), i.e. vertical.*

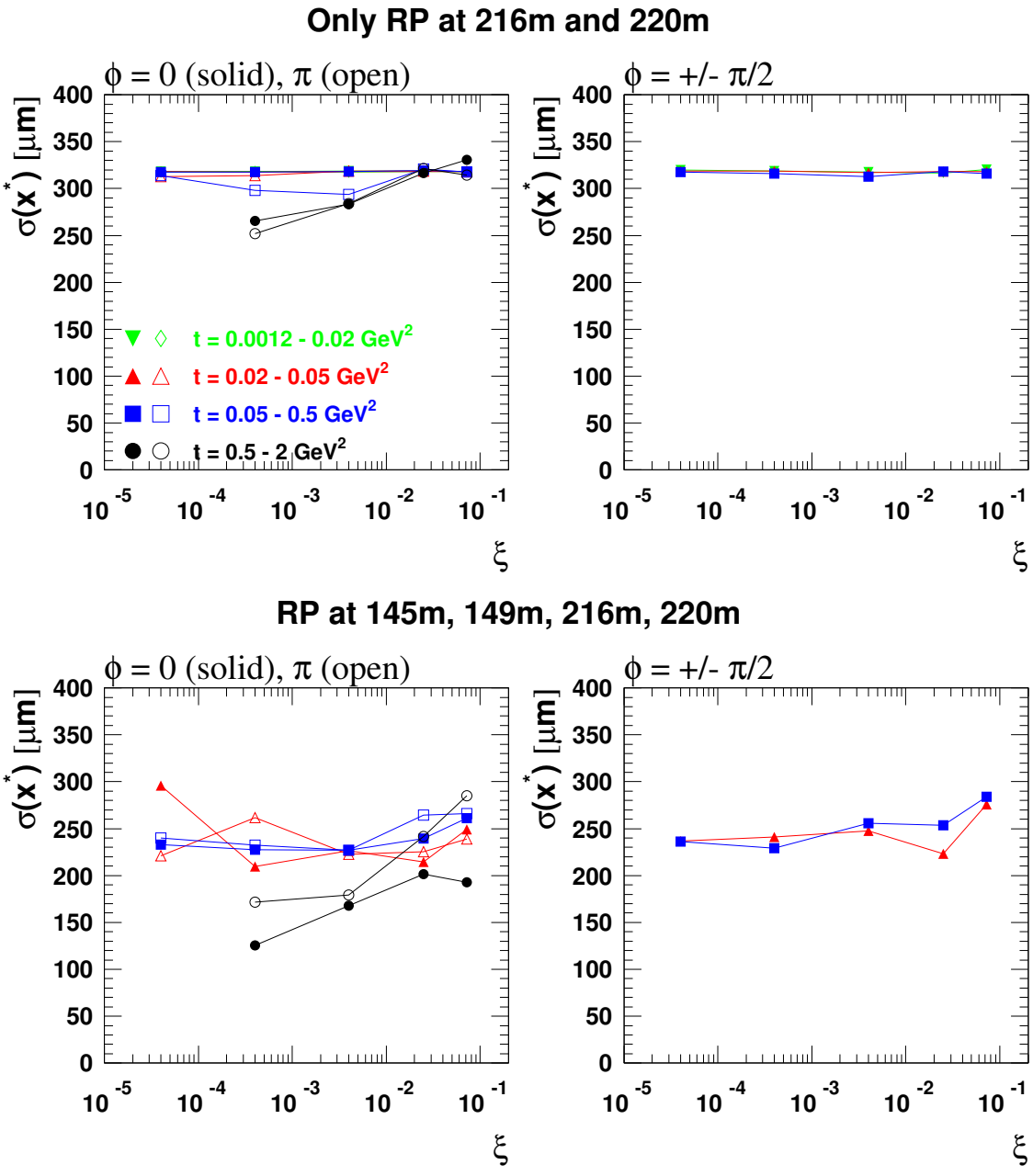

Figure 13: *x^* resolution with tracked protons as a function of ξ for different t and azimuthal angles: $\phi = 0, \pi$ (left-hand plots), i.e. horizontal, and $\phi = \pm\pi/2$ (right-hand plots), i.e. vertical. For clarity, the error bars (typically several tens of microns) have been omitted in this figure.*

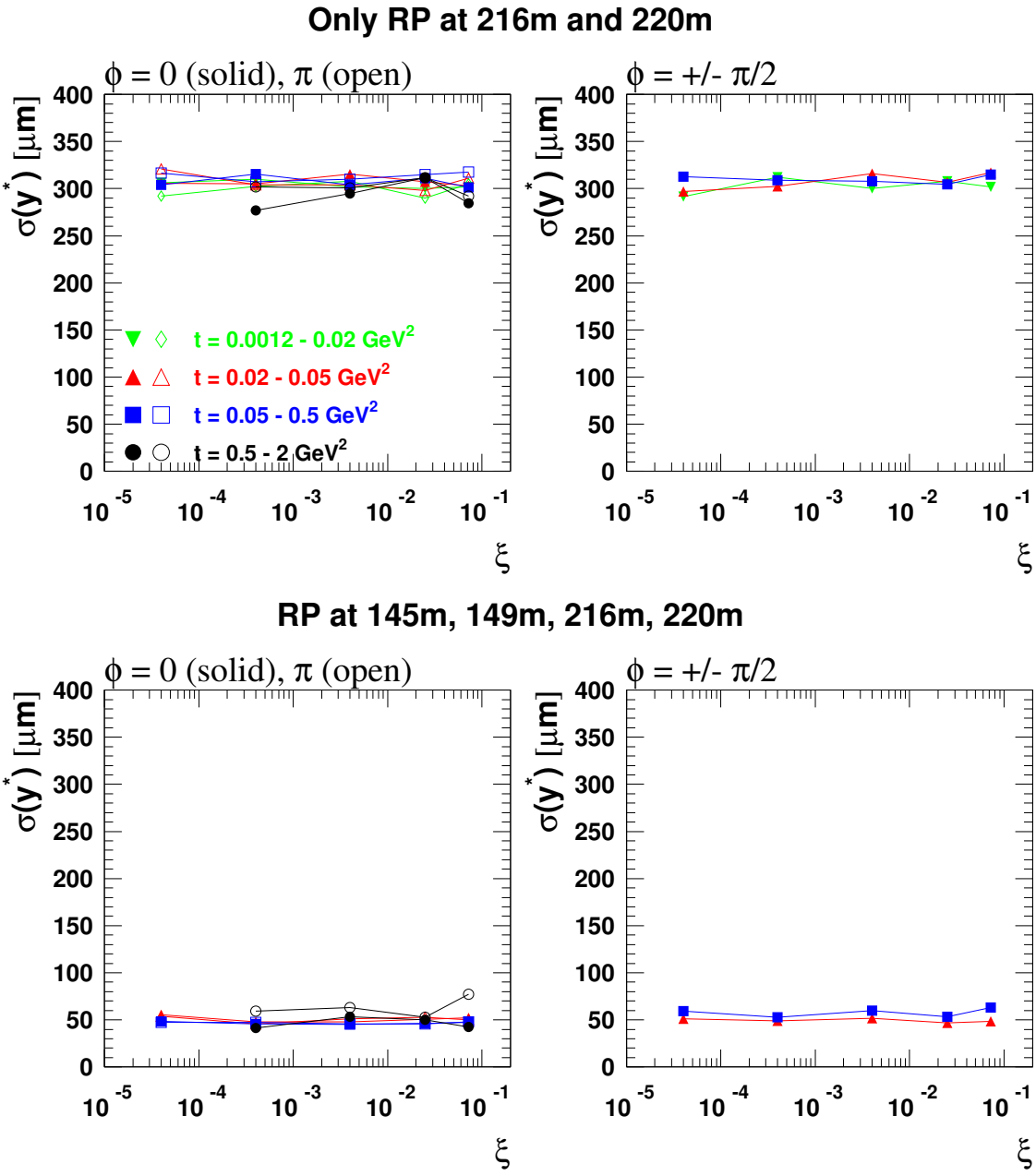

Figure 14: *y^* resolution with tracked protons as a function of ξ for different t and azimuthal angles: $\phi = 0, \pi$ (left-hand plots), i.e. horizontal, and $\phi = \pm\pi/2$ (right-hand plots), i.e. vertical.*

3.3 Double-Arm Reconstruction (DPE)

Since both protons come from the same vertex (x^*, y^*) it is advantageous to reconstruct them both in a combined fit rather than separately.

The single-arm reconstruction studies have already established that the performance is much worse if only the RPs at 216 m and 220 m are used. Hence the double-arm reconstruction studies have only been done with all 8 RP units. Again, the vertex served as additional (weak) constraint in the fit: $x_0 = y_0 = 0 \pm 0.32\,\text{mm}$.

3.3.1 Ideal Study with Perfectly Known Optics

The resolution improvement from correlating the two protons of DPE events via their common vertex was studied with perfectly known optics, following the same procedure as in Section 3.2.1.

First an example case with $t_1 = t_2$, $\xi_1 = \xi_2$, and $\phi_{1,2} = \pm\pi/2$ was investigated. Indeed, the resolutions for combined double-arm reconstruction are better than for single-arm reconstruction (Figure 15). This effect is much more pronounced for ξ than for t, and for small ξ.

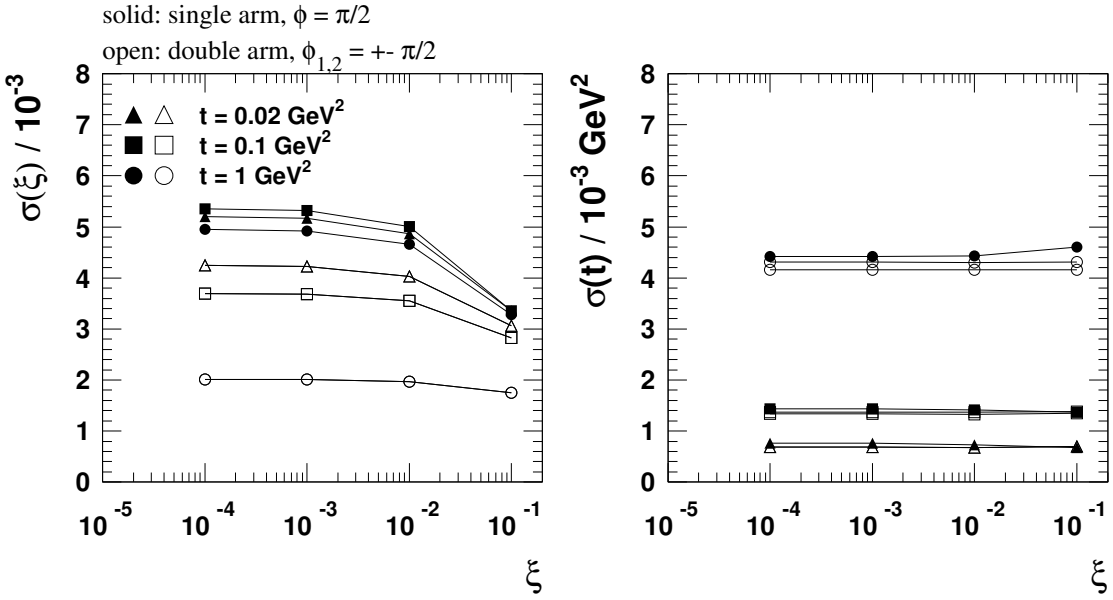

Figure 15: *Comparison of the ξ (left) and t (right) resolutions for single-arm and double-arm reconstruction with perfectly known optics. In the single-arm case, $\phi = \pi/2$ was chosen. In the double-arm case, this example shows a symmetric situation with two protons having $t_1 = t_2$, $\xi_1 = \xi_2$, and $\phi_{1,2} = \pm\pi/2$ respectively. The slight t-resolution differences between the two protons in the double-arm case are statistical.*

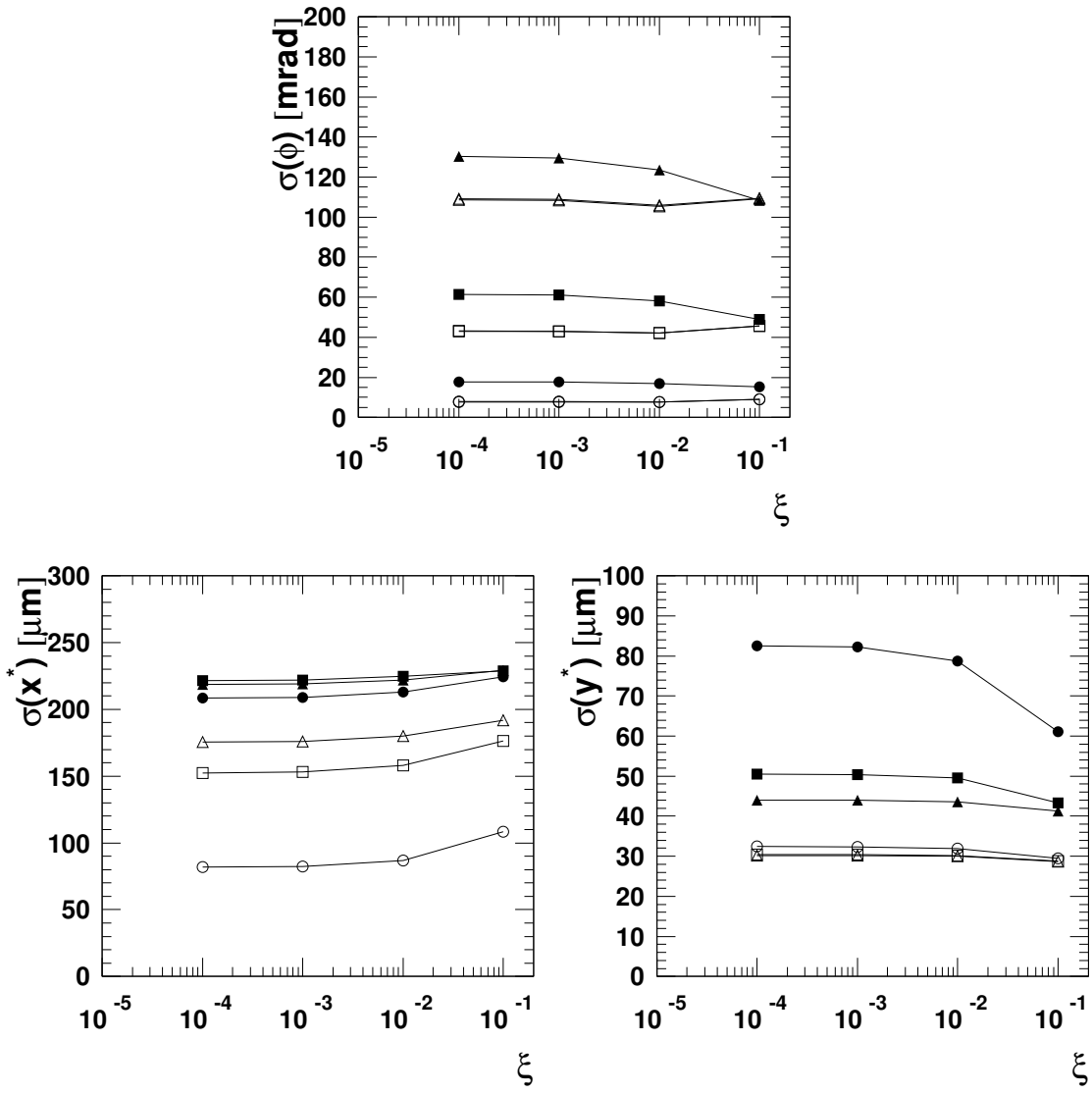

Figure 16: *Like Figure 15 but for the reconstructed ϕ (top) and the vertex position x^* (left) and y^* (right).*

The dependence of the resolution on the azimuthal emission angles of the two protons is shown in Figures 17 and 18. The study demonstrates that the azimuth of a given one of the two protons has a non-zero but very small impact on the resolution in the parameters of the other proton.

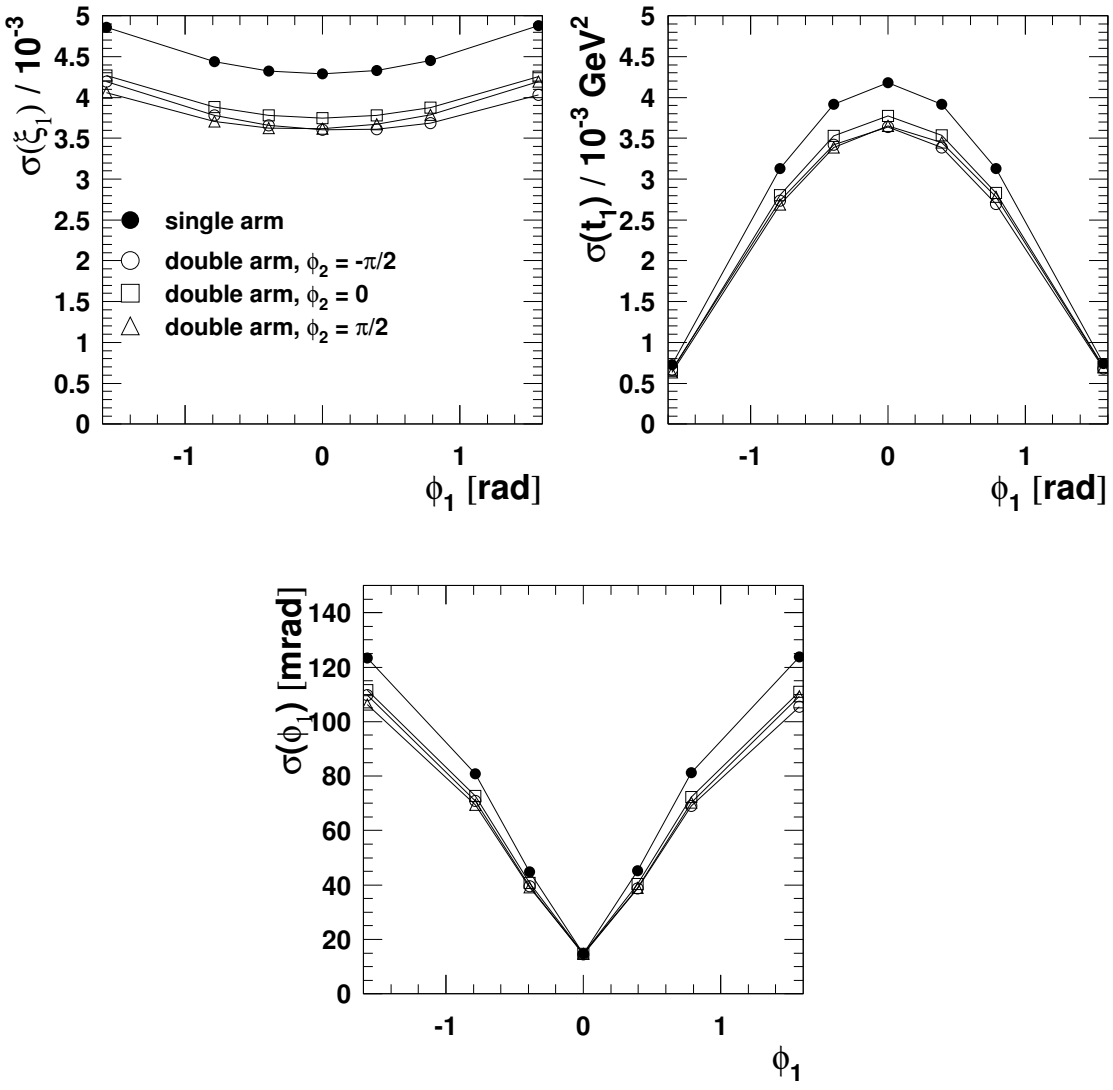

Figure 17: *Azimuthal dependence of the ξ (left), t (right) and ϕ (bottom) resolutions for single-arm and double-arm reconstruction with perfectly known optics. Shown is the resolution of the first proton as a function of its own azimuth for different values of the other proton's azimuth (in the double-arm case). In all cases, the protons have $t = 0.02\,\mathrm{GeV}^2$ and $\xi_1 = -10^{-2}$.*

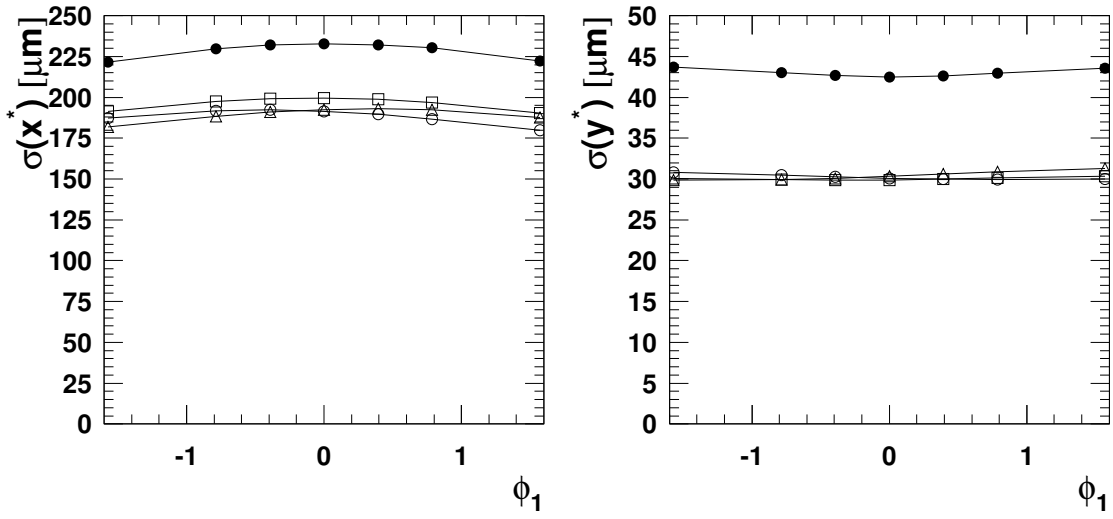

Figure 18: *Like Figure 17 but for the reconstructed vertex position x^* (left) and y^* (right).*

3.3.2 Study Based on Protons Tracked through the Machine

The final step was the full reconstruction of simulated DPE events with protons tracked through the machine. For each proton, detector acceptance was required. The parameter space studied was defined by the diffractive mass M and the ratio between the lower and the higher ξ-value of the two protons characterising the degree of momentum symmetry of the event. The binning scheme is shown in Figure 19. The other parameters, i.e. the t- and ϕ-values and the vertex coordinates were averaged. The reconstruction resolution for the various parameters is shown in Figures 20 and 21.

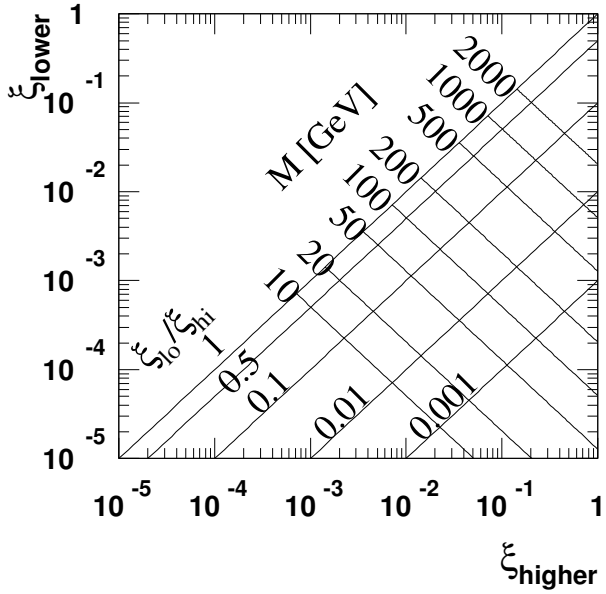

Figure 19: *Binning scheme of the double-arm resolution study for DPE events.*

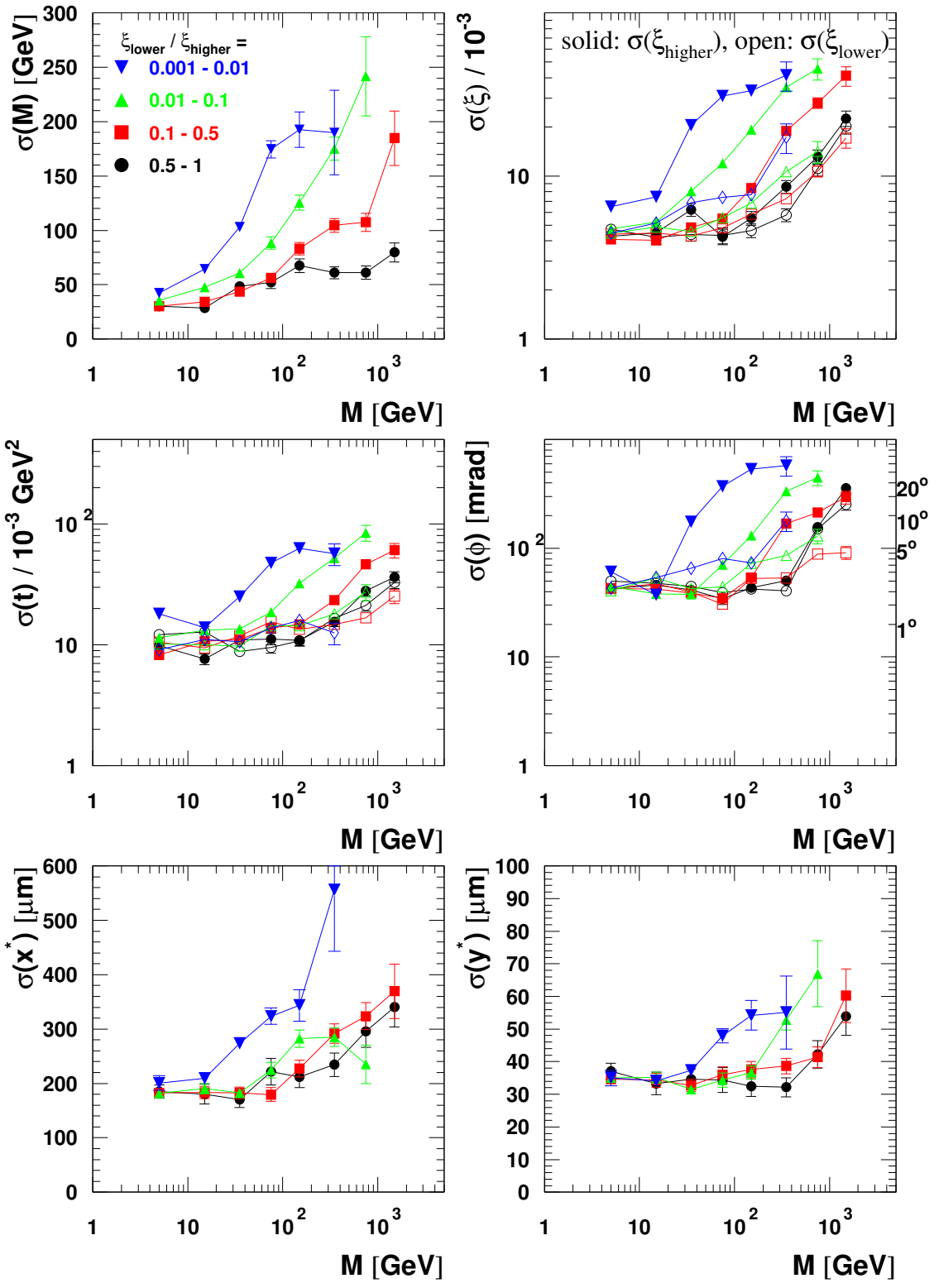

Figure 20: *Double-arm reconstruction study of DPE events. Resolution in the reconstructed kinematic parameters as a function of the diffractive mass for different ξ-ratios of the two protons (following the binning scheme of Figure 19.)*

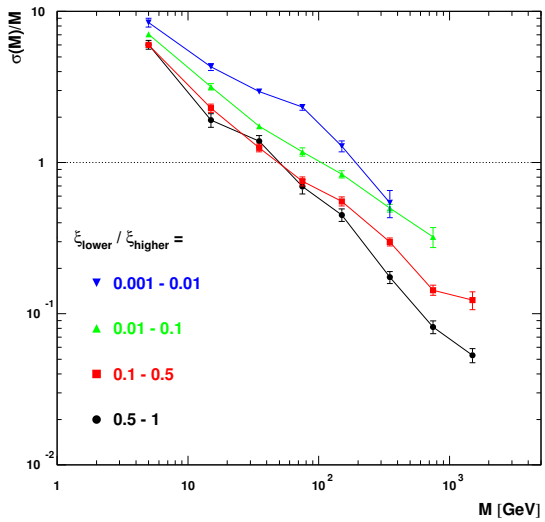

Figure 21: *Relative mass resolution for double-arm reconstruction study of DPE events.*

Note that for very asymmetric events and big masses one of the ξ-values is very large (e.g. at $M = 350\,\text{GeV}$ and $\xi_{lower}/\xi_{higher} = 0.005$: $\xi_{higher} = 0.35$, $\xi_{lower} = 0.0018$). In those regions the parameterisation is not accurate enough, leading to a bad reconstruction performance and large values of χ^2 (Figure 22).

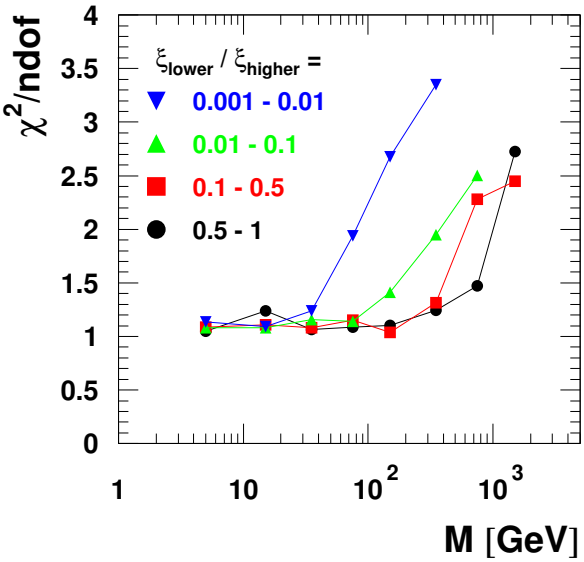

Figure 22: *Normalised χ^2 of the fits used in the DPE reconstruction discussed in the text and in Figure 20.*

References

[1] V. Avati, K. Österberg: Optical functions parametrization: $\beta^* = 1540\,\mathrm{m}$, TOTEM Internal Note 05-1.

[2] The CMS and TOTEM diffractive and forward physics working group: Prospects for Diffractive and Forward Physics at the LHC, CERN/LHCC 2006-039/G-124.

[3] V. Avati, K. Österberg: Acceptance calculation methods for β^*=0.5 m optics, TOTEM Internal Note 05-2.